

Supplementary materials

**Synthesis, Photophysical Properties and Application in Organic Light Emitting Devices of
Rhenium(I) Carbonyls incorporating Functionalized 2,2':6',2''-terpyridines**

Tomasz Klemens, Anna Świtlicka-Olszewska, Barbara Machura, Marzena Grucela, Henryk Janczek, Ewa Schab-Balcerzak, Agata Szlapa, Slawomir Kula, Stanisław Krompiec, Karolina Smolarek, Dorota Kowalska, Sebastian Mackowski, Karol Erfurt, Piotr Lodziński

Tables:	Page:
Table S1. Comparison of experimental and theoretical bond lengths [Å] and angles [°] for 1 , 3 , 4 and 6 .	3
Table S2. Short intra- and intermolecular contacts detected in the structures of the tricarbonyl rhenium(I) complexes.	4
Table S3. Frontier molecular orbital composition (%) in the ground state for complex 1 calculated at the DFT/B3LYP/DEF2-TZVPD/6-31+G* level.	5
Table S4. Frontier molecular orbital composition (%) in the ground state for complex 2 calculated at the DFT/B3LYP/DEF2-TZVPD/6-31+G* level.	5
Table S5. Frontier molecular orbital composition (%) in the ground state for complex 3 calculated at the DFT/B3LYP/DEF2-TZVPD/6-31+G* level.	5
Table S6. Frontier molecular orbital composition (%) in the ground state for complex 4 calculated at the DFT/B3LYP/DEF2-TZVPD/6-31+G* level.	6
Table S7. Frontier molecular orbital composition (%) in the ground state for complex 5 calculated at the DFT/B3LYP/DEF2-TZVPD/6-31+G* level.	6
Table S8. Frontier molecular orbital composition (%) in the ground state for complex 6 calculated at the DFT/B3LYP/DEF2-TZVPD/6-31+G* level.	6
Table S9. Frontier molecular orbital composition (%) in the ground state for complexes 2 , 3 , and 6 calculated at the DFT/B3LYP level using different basis sets.	7
Table S10. Main contributions to frontier molecular orbitals (%) in the ground state for complexes 2 , 3 , and 6 calculated at the DFT/B3LYP/TZ2P level using ADF software with ZORA relativistic approximation and COSMO solvent model.	7
Table S11. The energies and characters of the selected spin-allowed electronic transitions for 1 calculated with the TDDFT/B3LYP method, together with assignment to the experimental absorption bands.	8
Table S12. The energies and characters of the selected spin-allowed electronic transitions for 2 calculated with the TDDFT/B3LYP method, together with assignment to the experimental absorption bands.	9
Table S13. The energies and characters of the selected spin-allowed electronic transitions for 3 calculated with the TDDFT/B3LYP method, together with assignment to the experimental absorption bands.	10
Table S14. The energies and characters of the selected spin-allowed electronic transitions for 4 calculated with the TDDFT/B3LYP method, together with assignment to the experimental	10

absorption bands.

Table S15. The energies and characters of the selected spin-allowed electronic transitions for **5** calculated with the TDDFT/B3LYP method, together with assignment to the experimental absorption bands. 11

Table S16. The energies and characters of the selected spin-allowed electronic transitions for **6** calculated with the TDDFT/B3LYP method, together with assignment to the experimental absorption bands. 12

Table S17. The energies and characters of the of two lowest vertical electronic transitions for **6** complex obtained in TDDFT calculations with using different functionals. 13

Figures:	Page:
Figure S1. A view of the crystal packing showing intermolecular π - π stacking interactions for 1 and 6 . 14	
Figure S2. DSC thermograms of compound 2 . T_c : crystallization temperature; T_m melting point temperature; T_g glass transition temperature. 15	
Figure S3. Molecular orbital energy level graph of complexes 2 , 3 and 6 at the DFT/B3LYP level using different basis sets. 16	
Figure S4. Excitation and emission spectra together with PL lifetime curves for 1-6 in CHCl ₃ , MeCN, low-temperature MeOH:EtOH glass matrix and in solid state. 17-22	
Figure S5. Isodensity surface plots of the HSOMO and LSOMO for the complexes 1-6 at their T_1 state geometry calculated in MeCN medium at the TD-DFT/DFT/B3LYP level associated with the PCM model. Blue and grey colours show regions of positive and negative spin density values, respectively. 23-24	
Figure S6. AFM images (10 μm x 10 μm) of the blend PVK with compound 3 . 24	

Table S1. Comparison of experimental and theoretical bond lengths [Å] and angles [°] for **1**, **3**, **4** and **6**.

Bond lengths	Exp.	Opt.		Bond angles		Exp.	Opt.	
		S ₀	T ₁				S ₀	T ₁
1								
Re(1)–C(1)	1.905(5)	1.939	1.938	C(2)–Re(1)–C(1)	87.02(17)	86.82	87.24	
Re(1)–C(2)	1.899(5)	1.921	1.932	C(3)–Re(1)–C(1)	90.82(19)	91.11	90.83	
Re(1)–C(3)	1.919(5)	1.912	1.912	C(3)–Re(1)–C(2)	90.18(18)	89.85	89.64	
Re(1)–N(1)	2.160(3)	2.202	2.202	C(1)–Re(1)–N(1)	174.37(15)	174.51	174.68	
Re(1)–N(2)	2.216(3)	2.267	2.212	C(2)–Re(1)–N(1)	95.86(15)	96.79	96.45	
Re(1)–Cl(1)	2.4848(11)	2.549	2.565	C(3)–Re(1)–N(1)	94.00(15)	93.02	93.02	
C(1)–O(1)	1.154(5)	1.164	1.165	C(1)–Re(1)–N(2)	101.97(14)	101.71	100.88	
C(2)–O(2)	1.151(6)	1.167	1.166	C(2)–Re(1)–N(2)	168.64(14)	169.35	169.41	
C(3)–O(3)	1.121(5)	1.170	1.170	C(3)–Re(1)–N(2)	96.55(14)	96.28	96.98	
Re(2)–C(31)	1.918(5)			N(1)–Re(1)–N(2)	74.61(11)	74.25	75.02	
Re(2)–C(32)	1.881(5)			C(1)–Re(1)–Cl(1)	89.59(14)	91.13	91.26	
Re(2)–C(33)	1.902(5)			C(2)–Re(1)–Cl(1)	91.12(14)	91.27	89.56	
Re(2)–N(4)	2.164(3)			C(3)–Re(1)–Cl(1)	178.65(12)	177.55	177.71	
Re(2)–N(5)	2.216(3)			N(1)–Re(1)–Cl(1)	85.53(8)	84.68	84.94	
Re(2)–Cl(2)	2.4979(10)			N(2)–Re(1)–Cl(1)	82.11(8)	82.29	83.51	
C(31)–O(4)	1.150(5)			C(32)–Re(2)–C(31)	86.97(17)			
C(32)–O(5)	1.167(5)			C(33)–Re(2)–C(31)	87.85(18)			
C(33)–O(6)	1.144(5)			C(33)–Re(2)–C(32)	89.47(19)			
				C(31)–Re(2)–N(4)	175.63(15)			
				C(32)–Re(2)–N(4)	95.79(15)			
				C(33)–Re(2)–N(4)	95.54(15)			
				C(31)–Re(2)–N(5)	102.37(14)			
				C(32)–Re(2)–N(5)	168.94(14)			
				C(33)–Re(2)–N(5)	96.70(15)			
				N(4)–Re(2)–N(5)	74.54(11)			
				C(31)–Re(2)–Cl(2)	92.92(13)			
				C(32)–Re(2)–Cl(2)	92.51(15)			
				C(33)–Re(2)–Cl(2)	177.90(13)			
				N(4)–Re(2)–Cl(2)	83.60(8)			
				N(5)–Re(2)–Cl(2)	81.23(8)			
3								
Re(1)–C(1)	1.929(8)	1.937	1.977	C(2)–Re(1)–C(1)	86.5(3)	86.78	82.66	
Re(1)–C(2)	1.898(7)	1.919	1.982	C(3)–Re(1)–C(1)	93.7(3)	90.52	98.53	
Re(1)–C(3)	1.969(8)	1.915	1.986	C(3)–Re(1)–C(2)	90.7(3)	90.18	86.98	
Re(1)–N(1)	2.174(5)	2.202	2.161	C(1)–Re(1)–N(1)	175.3(2)	174.86	172.70	
Re(1)–N(2)	2.231(5)	2.265	2.143	C(2)–Re(1)–N(1)	95.1(2)	96.40	99.78	
Re(1)–Cl(1)	2.4650(18)	2.552	2.470	C(3)–Re(1)–N(1)	90.7(3)	93.50	88.49	
C(1)–O(1)	1.156(8)	1.164	1.156	C(1)–Re(1)–N(2)	103.2(2)	102.23	101.06	
C(2)–O(2)	1.156(8)	1.168	1.157	C(2)–Re(1)–N(2)	169.5(2)	169.34	175.24	
C(3)–O(3)	1.065(8)	1.169	1.153	C(3)–Re(1)–N(2)	92.7(2)	95.39	95.34	
				N(1)–Re(1)–N(2)	74.97(19)	74.24	76.16	
				C(1)–Re(1)–Cl(1)	91.0(2)	91.23	89.04	
				C(2)–Re(1)–Cl(1)	90.5(2)	91.82	88.56	
				C(3)–Re(1)–Cl(1)	175.2(2)	177.41	170.65	
				N(1)–Re(1)–Cl(1)	84.62(14)	84.64	84.17	
				N(2)–Re(1)–Cl(1)	85.39(13)	82.38	88.54	
4								
Re(1)–C(1)	1.919(9)	1.937	1.977	C(2)–Re(1)–C(1)	86.5(3)	86.76	82.66	
Re(1)–C(2)	1.894(8)	1.919	1.982	C(3)–Re(1)–C(1)	93.4(4)	90.52	98.56	
Re(1)–C(3)	1.950(9)	1.915	1.986	C(3)–Re(1)–C(2)	91.0(3)	90.19	86.96	
Re(1)–N(1)	2.164(6)	2.202	2.161	C(1)–Re(1)–N(1)	175.1(3)	174.86	172.66	
Re(1)–N(2)	2.227(6)	2.265	2.143	C(2)–Re(1)–N(1)	95.3(3)	96.42	99.80	
Re(1)–Cl(1)	2.459(2)	2.552	2.470	C(3)–Re(1)–N(1)	91.1(3)	93.49	88.51	
C(1)–O(1)	1.163(9)	1.164	1.156	C(1)–Re(1)–N(2)	102.9(3)	102.22	101.06	
C(2)–O(2)	1.162(9)	1.168	1.157	C(2)–Re(1)–N(2)	169.7(3)	169.35	175.20	
C(3)–O(3)	1.063(10)	1.169	1.153	C(3)–Re(1)–N(2)	92.5(3)	95.38	95.42	
				N(1)–Re(1)–N(2)	75.0(2)	74.24	76.14	
				C(1)–Re(1)–Cl(1)	91.0(2)	91.26	89.02	
				C(2)–Re(1)–Cl(1)	90.7(3)	91.82	88.53	

				C(3)–Re(1)–Cl(1) N(1)–Re(1)–Cl(1) N(2)–Re(1)–Cl(1)	175.4(3) 84.45(16) 85.13(15)	177.38 84.62 82.37	170.61 84.15 88.51
6							
Re(1)–C(1)	1.925(8)	1.939	1.938	C(2)–Re(1)–C(1)	87.9(3)	86.83	86.96
Re(1)–C(2)	1.922(7)	1.921	1.929	C(3)–Re(1)–C(1)	88.5(3)	91.05	91.02
Re(1)–C(3)	1.884(8)	1.912	1.905	C(3)–Re(1)–C(2)	88.6(3)	89.86	89.62
Re(1)–N(1)	2.173(6)	2.203	2.191	C(1)–Re(1)–N(1)	175.2(3)	174.57	174.39
Re(1)–N(2)	2.200(5)	2.262	2.210	C(2)–Re(1)–N(1)	96.1(3)	96.76	96.11
Re(1)–Cl(1)	2.4995(17)	2.552	2.590	C(3)–Re(1)–N(1)	94.1(3)	93.02	93.70
C(1)–O(1)	1.159(9)	1.164	1.167	C(1)–Re(1)–N(2)	101.7(2)	101.73	101.14
C(2)–O(2)	1.130(8)	1.167	1.169	C(2)–Re(1)–N(2)	168.4(2)	169.36	169.56
C(3)–O(3)	1.167(9)	1.170	1.173	C(3)–Re(1)–N(2)	98.1(3)	96.22	96.75
				N(1)–Re(1)–N(2)	74.03(19)	74.27	75.30
				C(1)–Re(1)–Cl(1)	93.6(2)	91.16	90.62
				C(2)–Re(1)–Cl(1)	91.8(2)	91.14	89.75
				C(3)–Re(1)–Cl(1)	177.8(2)	177.63	178.21
				N(1)–Re(1)–Cl(1)	83.71(14)	84.72	84.70
				N(2)–Re(1)–Cl(1)	81.12(13)	82.47	83.63

Table S2. Short intra- and intermolecular contacts detected in the structures of the rhenium(I) complexes.

D—H \cdots A	D—H	H \cdots A	D \cdots A [Å]	D—H \cdots A [°]
1				
C(7)–H(7) \cdots Cl(2)#1	0.93	2.72	3.599(3)	158.00
C(37)–H(37) \cdots Cl(1)#2	0.93	2.71	3.593(3)	158.00
C(50)–H(50) \cdots Cl(1)#2	0.93	2.82	3.668(4)	153.00
C(57)–H(57) \cdots O(1)#3	0.93	2.50	3.344(6)	151.00
C(60)–H(60) \cdots Cl(2)#3	0.93	2.68	3.582(5)	163.00
3				
C(7)–H(7) \cdots Cl(1)#4	0.93	2.76	3.602(8)	151.00
C(17)–H(17) \cdots Cl(1)#1	0.93	2.76	3.534(8)	142.00
4				
C(7)–H(7) \cdots Cl(1)#5	0.93	2.77	3.609(8)	151.00
C(17)–H(17) \cdots Cl(1)#1	0.93	2.77	3.541(9)	141.00
C(20)–H(20) \cdots Cl(1)#5	0.93	2.82	3.728(10)	165.00

Symmetry codes: #1: -1+x,y,z; #2: 1+x,y,z; #3: 2-x,1-y,1-z; #4: x,1/2-y,-1/2+z; #5: x,3/2-y,-1/2+z

Table S3. Frontier molecular orbital composition (%) in the ground state for complex **1** calculated at the DFT/B3LYP/DEF2-TZVPD/6-31+G* level.

Orbital	Energy [eV]	Contribution (%)					Character
		Re	3CO	Cl	R	terpy	
LUMO+5	-0.99	30.36	28.97	2.66	15.89	22.13	$d(Re) + \pi^*(CO) + \pi^*(terpy) + \pi^*(R)$
LUMO+4	-1.03	11.90	26.99	6.99	8.07	46.06	$d(Re) + \pi^*(CO) + \pi^*(terpy)$
LUMO+3	-1.27	14.41	12.70	0.49	10.23	62.17	$\pi^*(terpy) + d(Re) + \pi^*(CO) + \pi^*(R)$
LUMO+2	-1.56	13.18	4.99	2.07	4.52	75.24	$\pi^*(terpy) + d(Re)$
LUMO+1	-1.96	2.69	1.60	0.60	14.53	80.58	$\pi^*(terpy) + \pi^*(R)$
LUMO	-2.64	10.86	3.51	2.76	8.24	74.63	$\pi^*(terpy) + d(Re)$
HOMO	-6.23	16.17	9.46	5.66	57.11	11.61	$\pi(R) + d(Re)$
HOMO-1	-6.33	41.31	23.91	21.28	6.68	6.82	$d(Re) + \pi(CO) + p(Cl)$
HOMO-2	-6.48	32.47	19.65	22.99	18.54	6.35	$d(Re) + \pi(CO) + p(Cl) + \pi(R)$
HOMO-3	-6.75	54.28	30.95	1.57	0.16	13.04	$d(Re) + \pi(CO)$
HOMO-4	-6.97	0.01	0.00	0.00	99.93	0.06	$\pi(R)$
HOMO-5	-7.12	3.25	2.72	0.12	4.17	89.74	$\pi(terpy)$

Table S4. Frontier molecular orbital composition (%) in the ground state for complex **2** calculated at the DFT/B3LYP/DEF2-TZVPD/6-31+G* level.

Orbital	Energy [eV]	Contribution (%)					Character
		Re	3CO	Cl	R	terpy	
LUMO+5	-1.01	31.23	31.60	0.87	7.34	28.95	$d(Re) + \pi^*(CO) + \pi^*(terpy)$
LUMO+4	-1.04	9.75	15.79	5.34	10.72	58.40	$\pi^*(terpy) + \pi^*(CO) + \pi^*(R)$
LUMO+3	-1.26	8.37	3.72	0.30	37.28	50.33	$\pi^*(terpy) + \pi^*(R)$
LUMO+2	-1.52	7.89	4.27	1.65	4.68	81.51	$\pi^*(terpy)$
LUMO+1	-1.89	1.12	1.19	0.45	15.00	82.24	$\pi^*(terpy) + \pi^*(R)$
LUMO	-2.59	13.75	3.43	3.11	5.76	73.95	$\pi^*(terpy) + d(Re)$
HOMO	-5.80	1.86	1.23	0.40	84.97	11.54	$\pi(R) + \pi(terpy)$
HOMO-1	-6.25	44.24	26.70	21.87	0.64	6.54	$d(Re) + \pi(CO) + p(Cl)$
HOMO-2	-6.39	41.91	24.58	24.15	2.52	6.83	$d(Re) + \pi(CO) + p(Cl)$
HOMO-3	-6.71	56.57	32.17	1.59	0.04	9.63	$d(Re) + \pi(CO)$
HOMO-4	-6.95	0.56	0.03	0.01	97.51	1.89	$\pi(R)$
HOMO-5	-7.11	1.31	1.38	0.25	2.29	94.77	$\pi(terpy)$

Table S5. Frontier molecular orbital composition (%) in the ground state for complex **3** calculated at the DFT/B3LYP/DEF2-TZVPD/6-31+G* level.

Orbital	Energy [eV]	Contribution (%)					Character
		Re	3CO	Cl	R	terpy	
LUMO+5	-0.92	30.06	34.32	6.59	7.81	21.22	$d(Re) + \pi^*(CO) + \pi^*(terpy)$
LUMO+4	-1.04	23.95	23.84	2.49	0.99	48.74	$\pi^*(terpy) + d(Re) + \pi^*(CO)$
LUMO+3	-1.21	11.06	8.46	0.89	9.08	70.52	$\pi^*(terpy) + d(Re)$
LUMO+2	-1.54	9.25	4.43	1.84	3.34	81.13	$\pi^*(terpy)$
LUMO+1	-1.97	0.99	1.18	0.38	13.86	83.59	$\pi^*(terpy) + \pi^*(R)$
LUMO	-2.67	10.92	3.44	2.95	7.96	74.74	$\pi^*(terpy) + d(Re)$
HOMO	-6.25	44.13	26.90	21.70	0.57	6.70	$d(Re) + \pi(CO) + p(Cl)$
HOMO-1	-6.38	42.20	24.37	21.69	3.74	7.99	$d(Re) + \pi(CO) + p(Cl)$
HOMO-2	-6.72	56.31	31.85	1.73	0.24	9.87	$d(Re) + \pi(CO)$
HOMO-3	-6.95	2.08	0.91	6.85	72.77	17.39	$\pi(R) + \pi(terpy)$
HOMO-4	-7.16	1.13	1.44	0.26	1.29	95.87	$\pi(terpy)$
HOMO-5	-7.50	1.04	0.05	0.03	94.89	3.98	$\pi(R)$

Table S6. Frontier molecular orbital composition (%) in the ground state for complex **4** calculated at the DFT/B3LYP/DEF2-TZVPD/6-31+G* level.

Orbital	Energy [eV]	Contribution (%)					Character
		Re	3CO	Cl	R	terpy	
LUMO+5	-0.92	29.91	34.31	6.39	8.22	21.16	d(Re) + $\pi^*(\text{CO}) + \pi^*(\text{terpy})$
LUMO+4	-1.04	23.71	23.66	2.57	1.06	48.99	$\pi^*(\text{terpy}) + d(\text{Re}) + \pi^*(\text{CO})$
LUMO+3	-1.21	10.93	8.10	0.83	9.51	70.63	$\pi^*(\text{terpy}) + d(\text{Re})$
LUMO+2	-1.55	9.20	4.43	1.85	3.46	81.06	$\pi^*(\text{terpy})$
LUMO+1	-1.98	0.99	1.18	0.37	14.08	83.38	$\pi^*(\text{terpy}) + \pi^*(\text{R})$
LUMO	-2.68	10.94	3.43	2.95	8.03	74.66	$\pi^*(\text{terpy}) + d(\text{Re})$
HOMO	-6.26	44.11	26.89	21.71	0.61	6.69	d(Re) + $\pi(\text{CO}) + p(\text{Cl})$
HOMO-1	-6.38	42.03	24.26	21.60	4.13	7.98	d(Re) + $\pi(\text{CO}) + p(\text{Cl})$
HOMO-2	-6.72	56.22	31.80	1.75	0.36	9.87	d(Re) + $\pi(\text{CO})$
HOMO-3	-6.90	2.26	1.05	6.01	75.72	14.95	$\pi(\text{R}) + \pi(\text{terpy})$
HOMO-4	-7.16	1.13	1.45	0.26	1.25	95.91	$\pi(\text{terpy})$
HOMO-5	-7.51	1.04	0.05	0.03	94.91	3.96	$\pi(\text{R})$

Table S7. Frontier molecular orbital composition (%) in the ground state for complex **5** calculated at the DFT/B3LYP/DEF2-TZVPD/6-31+G* level.

Orbital	Energy [eV]	Contribution (%)					Character
		Re	3CO	Cl	R	terpy	
LUMO+5	-0.92	32.97	28.48	6.17	12.38	20.00	d(Re) + $\pi^*(\text{CO}) + \pi^*(\text{terpy}) + \pi^*(\text{R})$
LUMO+4	-1.04	24.86	25.10	2.19	0.49	47.36	$\pi^*(\text{terpy}) + d(\text{Re}) + \pi^*(\text{CO})$
LUMO+3	-1.20	12.49	8.51	0.99	8.80	69.21	$\pi^*(\text{terpy}) + d(\text{Re})$
LUMO+2	-1.55	8.12	4.41	1.79	2.55	83.14	$\pi^*(\text{terpy})$
LUMO+1	-1.98	1.10	1.19	0.31	11.04	86.37	$\pi^*(\text{terpy}) + \pi^*(\text{R})$
LUMO	-2.69	12.61	3.32	2.99	7.07	74.01	$\pi^*(\text{terpy}) + d(\text{Re})$
HOMO	-6.26	44.27	26.86	21.94	0.31	6.61	d(Re) + $\pi(\text{CO}) + p(\text{Cl})$
HOMO-1	-6.39	42.73	24.82	22.93	2.10	7.42	d(Re) + $\pi(\text{CO}) + p(\text{Cl})$
HOMO-2	-6.73	56.52	31.93	1.58	0.06	9.91	d(Re) + $\pi(\text{CO})$
HOMO-3	-7.14	1.03	0.40	7.72	69.38	21.47	$\pi(\text{R}) + \pi(\text{terpy})$
HOMO-4	-7.18	1.18	1.41	0.59	3.57	93.25	$\pi(\text{terpy})$
HOMO-5	-7.56	1.15	0.36	3.68	68.22	26.59	$\pi(\text{R}) + \pi(\text{terpy})$

Table S8. Frontier molecular orbital composition (%) in the ground state for complex **6** calculated at the DFT/B3LYP/DEF2-TZVPD/6-31+G* level.

Orbital	Energy [eV]	Contribution (%)					Character
		Re	3CO	Cl	R	terpy	
LUMO+5	-0.77	16.55	25.25	2.86	0.31	55.03	$\pi^*(\text{terpy}) + d(\text{Re}) + \pi^*(\text{CO})$
LUMO+4	-0.99	21.71	36.99	8.47	0.20	32.63	d(Re) + $\pi^*(\text{CO}) + \pi^*(\text{terpy})$
LUMO+3	-1.18	22.53	19.23	0.84	2.43	54.98	$\pi^*(\text{terpy}) + d(\text{Re}) + \pi^*(\text{CO})$
LUMO+2	-1.49	12.87	4.70	1.81	2.16	78.45	$\pi^*(\text{terpy}) + d(\text{Re})$
LUMO+1	-1.80	3.59	1.80	0.82	10.48	83.31	$\pi^*(\text{terpy}) + \pi^*(\text{R})$
LUMO	-2.51	9.98	3.78	2.79	7.33	76.12	$\pi^*(\text{terpy})$
HOMO	-5.41	3.87	0.92	0.39	81.84	12.98	$\pi(\text{R}) + \pi(\text{terpy})$
HOMO-1	-6.29	43.67	26.86	22.73	0.40	6.34	d(Re) + $\pi(\text{CO}) + p(\text{Cl})$
HOMO-2	-6.42	41.60	24.49	24.50	2.31	7.09	d(Re) + $\pi(\text{CO}) + p(\text{Cl})$
HOMO-3	-6.72	54.00	30.89	1.59	0.10	13.42	d(Re) + $\pi(\text{CO})$
HOMO-4	-7.02	3.27	2.48	0.11	16.69	77.45	$\pi(\text{terpy}) + \pi(\text{R})$
HOMO-5	-7.11	0.86	0.55	0.04	77.52	21.03	$\pi(\text{R}) + \pi(\text{terpy})$

Table S9. Frontier molecular orbital composition (%) in the ground state for complexes **2**, **3**, and **6** calculated at the DFT/B3LYP level using different basis sets.

Compound	Basis Set	Orbital	Energy [eV]	Contribution (%)					Character
				Re	3CO	Cl	R	terpy	
2	def2-TZVPD/ 6-31+g*	LUMO	-2.59	13.75	3.43	3.11	5.76	73.95	$\pi^*(\text{terpy}) + d(\text{Re})$
		HOMO	-5.80	1.86	1.23	0.40	84.97	11.54	$\pi(\text{R}) + \pi(\text{terpy})$
		HOMO-1	-6.25	44.24	26.70	21.87	0.64	6.54	$d(\text{Re}) + \pi(\text{CO}) + p(\text{Cl})$
	TZVP	LUMO	-2.71	2.68	1.86	0.73	9.87	84.86	$\pi^*(\text{terpy})$
		HOMO	-6.01	4.34	2.68	0.61	54.16	38.21	$\pi(\text{R}) + \pi(\text{terpy})$
		HOMO-1	-6.21	38.06	22.51	11.20	9.20	19.03	$d(\text{Re}) + \pi(\text{CO}) + p(\text{Cl}) + \pi(\text{terpy})$
	def2TZVPD	LUMO	-2.70	7.72	9.57	0.92	6.47	75.32	$\pi^*(\text{terpy})$
		HOMO	-5.99	4.83	3.05	0.80	72.50	18.83	$\pi(\text{R}) + \pi(\text{terpy})$
		HOMO-1	-6.21	49.19	25.13	16.62	2.05	7.02	$d(\text{Re}) + \pi(\text{CO}) + p(\text{Cl})$
3				Re	3CO	Cl	R	terpy	
	def2-TZVPD/ 6-31+g*	LUMO	-2.67	10.92	3.44	2.95	7.96	74.74	$\pi^*(\text{terpy}) + d(\text{Re})$
		HOMO	-6.25	44.13	26.90	21.70	0.57	6.70	$d(\text{Re}) + \pi(\text{CO}) + p(\text{Cl})$
		HOMO-1	-6.38	42.20	24.37	21.69	3.74	7.99	$d(\text{Re}) + \pi(\text{CO}) + p(\text{Cl})$
	TZVP	LUMO	-2.79	2.69	1.84	0.67	8.75	86.05	$\pi^*(\text{terpy})$
		HOMO	-6.21	43.44	26.56	12.48	1.14	16.38	$d(\text{Re}) + \pi(\text{CO}) + p(\text{Cl}) + \pi(\text{terpy})$
		HOMO-1	-6.34	44.32	19.56	14.93	2.99	18.19	$d(\text{Re}) + \pi(\text{CO}) + p(\text{Cl}) + \pi(\text{terpy})$
	def2TZVPD	LUMO	-2.78	6.28	7.63	0.90	7.66	77.54	$\pi^*(\text{terpy})$
		HOMO	-6.21	50.39	26.08	16.51	0.37	6.65	$d(\text{Re}) + \pi(\text{CO}) + p(\text{Cl})$
		HOMO-1	-6.34	45.85	23.78	18.64	2.33	9.40	$d(\text{Re}) + \pi(\text{CO}) + p(\text{Cl})$
6				Re	3CO	Cl	R	terpy	
	def2-TZVPD/ 6-31+g*	LUMO	-2.51	9.98	3.78	2.79	7.33	76.12	$\pi^*(\text{terpy})$
		HOMO	-5.41	3.87	0.92	0.39	81.84	12.98	$\pi(\text{R}) + \pi(\text{terpy})$
		HOMO-1	-6.29	43.67	26.86	22.73	0.40	6.34	$d(\text{Re}) + \pi(\text{CO}) + p(\text{Cl})$
	TZVP	LUMO	-2.63	2.06	1.48	0.57	15.09	80.81	$\pi^*(\text{terpy}) + \pi^*(\text{R})$
		HOMO	-5.57	1.72	1.11	0.17	49.49	47.51	$\pi(\text{R}) + \pi(\text{terpy})$
		HOMO-1	-6.24	40.40	24.97	11.88	2.63	20.13	$d(\text{Re}) + \pi(\text{CO}) + p(\text{Cl}) + \pi(\text{terpy})$
	def2TZVPD	LUMO	-2.63	8.50	10.66	0.91	12.44	67.50	$\pi^*(\text{terpy}) + \pi^*(\text{R}) + \pi^*(\text{CO})$
		HOMO	-5.57	2.05	1.43	0.34	81.33	14.85	$\pi(\text{R}) + \pi(\text{terpy})$
		HOMO-1	-6.24	49.71	25.10	16.84	0.49	7.87	$d(\text{Re}) + \pi(\text{CO}) + p(\text{Cl})$

Table S10. Main contributions to frontier molecular orbitals (%) in the ground state for complexes **2**, **3**, and **6** calculated at the DFT/B3LYP/TZ2P level using ADF software with ZORA relativistic approximation and COSMO solvent model.

Compound	MO orbital	Energy [eV]	Main contribution
2	LUMO	-2.82	$\pi_{\text{terpy}}^*(91.84\%)$
	HOMO	-6.08	$\pi_{\text{R}}(81.92\%)$
	HOMO-1	-6.37	$d_{\text{Re}}(49.76\%) + \pi_{\text{CO}}(20.60\%) + p_{\text{Cl}}(18.56\%)$
3	LUMO	-2.88	$\pi_{\text{terpy}}^*(80.51\%)$
	HOMO	-6.36	$d_{\text{Re}}(50.61\%) + \pi_{\text{CO}}(18.06\%) + p_{\text{Cl}}(18.34\%)$
	HOMO-1	-6.49	$d_{\text{Re}}(46.43\%) + \pi_{\text{CO}}(18.22\%) + p_{\text{Cl}}(19.47\%)$
6	LUMO	-2.74	$\pi_{\text{terpy}}^*(86.41\%)$
	HOMO	-5.63	$\pi_{\text{R}}(83.94\%)$
	HOMO-1	-6.42	$d_{\text{Re}}(49.44\%) + \pi_{\text{CO}}(20.76\%) + p_{\text{Cl}}(16.77\%)$

Table S11. The energies and characters of the selected spin-allowed electronic transitions for **1** calculated with the TDDFT/B3LYP method, together with assignment to the experimental absorption bands.

Experimental absorption λ ; nm ($10^{-3} \epsilon$; M ⁻¹ cm ⁻¹)	Calculated transitions				
	Major contribution (%)	Character	E [eV]	λ [nm]	Oscillator strength
383.9 (8.7)	H-1 → L (65%)	MLCT/LLCT	2.93	422.66	0.0237
	H → L (41%)	ILCT/IL	3.07	403.65	0.2998
	H-2 → L (64%)	MLCT/LLCT/ILCT	3.31	375.02	0.2051
	H-3 → L (91%)	MLCT	3.36	369.38	0.0157
315.0 (37.9)	H → L+1 (52%)	ILCT	3.70	335.58	0.0933
	H-5 → L (64%)	ILCT	3.90	317.63	0.2001
	H-2 → L+1 (72%)	MLCT/LLCT	3.95	313.75	0.2063
	H-1 → L+2 (30%)	MLCT/LLCT	4.02	308.36	0.0624
	H → L+2 (23%)	ILCT			
278.6 (28.4)	H-9 → L (25%)	IL/LLCT	4.39	282.34	0.1031
	H-10 → L (23%)	LLCT/IL			
	H-3 → L+2 (12%)	MLCT			
	H-2 → L+2 (26%)	MLCT/LLCT/ILCT	4.42	280.64	0.0606
	H-3 → L+2 (24%)	MLCT			
	H → L+2 (19%)	ILCT			
	H → L+3 (36%)	ILCT	4.62	268.67	0.3036
	H-5 → L+1 (13%)	IL/ILCT			
	H-11 → L (29%)	LLCT/ILCT/IL	4.65	266.58	0.0775
	H-5 → L+1 (21%)	IL/ILCT			
191.49 (126.9)	H-11 → L (33%)	LLCT/ILCT/IL	4.72	262.64	0.1188
	H-5 → L+1 (12%)	IL/ILCT			
	H-15 → L+1 (14%)	IL	6.22	199.42	0.0531
	H-14 → L+1 (14%)	IL/ILCT			
	H → L+14 (15%)	LMCT/ILCT	6.31	196.57	0.0557
	H-2 → L+15 (11%)	d-d/LLCT/ILCT			
	H-6 → L+7 (26%)	IL/ILCT	6.34	195.68	0.0405
	H-6 → L+10 (19%)	IL			
	H-10 → L+6 (17%)	LLCT/IL	6.36	195.01	0.0411
	H-5 → L+9 (11%)	LLCT/IL	6.39	194.14	0.0489
	H-7 → L+7 (45%)	LLCT/ILCT/IL	6.46	191.86	0.0446

ϵ – molar absorption coefficient; H – highest occupied molecular orbital; L – lowest unoccupied molecular orbital

Table S12. The energies and characters of the selected spin-allowed electronic transitions for **2** calculated with the TDDFT/B3LYP method, together with assignment to the experimental absorption bands.

Experimental absorption λ ; nm ($10^{-3} \epsilon$; M ⁻¹ cm ⁻¹)	Calculated transitions				
	Major contribution (%)	Character	E [eV]	λ [nm]	Oscillator strength
374.0 (42.3)	H → L (97%)	ILCT/IL	2.74	453.34	0.1923
	H-2 → L (97%)	MLCT/LLCT	3.14	395.29	0.0391
	H → L+1 (98%)	ILCT	3.38	366.88	0.1729
306.0 (90.7)	H-5 → L (57%)	IL	3.95	314.02	0.1443
	H-1 → L+2 (57%)	MLCT/LLCT	4.04	307.31	0.1263
	H → L+3 (57%)	ILCT	4.10	302.80	0.0805
230.7 (184)	H-5 → L+1 (36%)	IL/ILCT	4.75	261.19	0.1144
	H-7 → L+1 (17%)	IL/ILCT			
	H-8 → L+1 (34%)	IL/LLCT/ILCT	5.09	243.74	0.0765
	H-7 → L+1 (12%)	IL/ILCT			
	H-12 → L (47%)	LLCT/ILCT/IL	5.19	239.05	0.0688
	H-13 → L (34%)	LLCT/ILCT/IL	5.38	230.64	0.1315
	H-4 → L+3 (27%)	ILCT/IL			
	H-5 → L+5 (18%)	LMCT/IL	5.50	225.56	0.0991
	H-7 → L+2 (17%)	IL			
206.35 (235.1)	H-10 → L+3 (15%)	LLCT/IL/ILCT	6.13	202.22	0.0692
	H-4 → L+7 (12%)	IL/ILCT			
	H-11 → L+2 (18%)	IL	6.22	199.27	0.0960
	H-7 → L+8 (12%)	IL/ILCT			
	H → L+14 (14%)	LMCT/ILCT	6.26	198.05	0.0788
	H-14 → L+1 (13%)	IL/ILCT			
	H-6 → L+7 (13%)	IL/ILCT			
	H-12 → L+2 (44%)	LLCT/ILCT	6.27	197.80	0.0817
	H-11 → L+2 (25%)	IL			

ϵ – molar absorption coefficient; H – highest occupied molecular orbital; L – lowest unoccupied molecular orbital

Table S13. The energies and characters of the selected spin-allowed electronic transitions for **3** calculated with the TDDFT/B3LYP method, together with assignment to the experimental absorption bands.

Experimental absorption λ ; nm ($10^{-3} \epsilon$; M ⁻¹ cm ⁻¹)	Calculated transitions				
	Major contribution (%)	Character	E [eV]	λ [nm]	Oscillator strength
385.4 (3.3)	H-1 → L (98%)	MLCT/LLCT	3.05	406.77	0.1248
	H-3 → L (80%)	ILCT	3.79	327.31	0.3658
284.9 (19.6)	H → L+2 (57%)	MLCT/LLCT	4.01	309.38	0.1121
	H-2 → L+2 (54%)	MLCT	4.40	281.81	0.0643
	H-3 → L+1 (63%)	ILCT	4.42	280.68	0.2227
	H-9 → L (68%)	LLCT/IL	4.49	275.98	0.0661
264.0 (18.2)	H-4 → L+1 (58%)	IL/ILCT	4.72	262.49	0.1216
	H-2 → L+4 (28%)	MLCT	4.76	260.39	0.0763
	H-2 → L+3 (18%)	MLCT			
196.6 (178.2)	H-3 → L+6 (56%)	ILCT	5.75	215.48	0.0517
	H-17 → L (23%)	IL/ILCT	5.92	209.60	0.0535
	H-15 → L (16%)	IL/ILCT/LLCT			
	H-11 → L+1 (13%)	LLCT/ILCT			
	H-12 → L+1 (24%)	IL/ILCT	6.24	198.80	0.0444
	H-3 → L+8 (23%)	ILCT			
	H-11 → L+2 (59%)	LLCT	6.29	197.21	0.0564
	H-5 → L+6 (32%)	ILCT	6.43	192.99	0.0441
	H-6 → L+7 (23%)	ILCT/IL			
	H-18 → L (15%)	ILCT/IL	6.46	191.90	0.0453
	H-16 → L+1 (13%)	IL			
	H-9 → L+6 (11%)	LLCT/IL/ILCT			

ϵ – molar absorption coefficient; H – highest occupied molecular orbital; L – lowest unoccupied molecular orbital

Table S14. The energies and characters of the selected spin-allowed electronic transitions for **4** calculated with the TDDFT/B3LYP method, together with assignment to the experimental absorption bands.

Experimental absorption λ ; nm ($10^{-3} \epsilon$; M ⁻¹ cm ⁻¹)	Calculated transitions				
	Major contribution (%)	Character	E [eV]	λ [nm]	Oscillator strength
385.4 (5.4)	H-1 → L (98%)	MLCT/LLCT	3.04	407.28	0.1295
	H-3 → L (70%)	ILCT	3.74	331.34	0.2269
	H-1 → L+1 (75%)	MLCT/LLCT	3.76	329.85	0.1538
294.5 (32.5)	H-4 → L (59%)	IL	3.91	317.10	0.1073
	H → L+2 (59%)	MLCT/LLCT	4.01	309.56	0.1078
	H-3 → L+1 (60%)	ILCT	4.38	283.40	0.2062
264.7 (30.8)	H-9 → L (69%)	LLCT/IL	4.48	276.70	0.0597
	H-4 → L+1 (68%)	IL/ILCT	4.72	262.74	0.1510
	H-2 → L+4 (28%)	MLCT	4.76	260.46	0.0742
	H-2 → L+3 (18%)	MLCT			
194.5 (71.8)	H-15 → L (19%)	IL/ILCT	5.91	209.97	0.0578
	H-12 → L+1 (13%)	LLCT			
	H-13 → L+1 (53%)	ILCT/LLCT/IL	6.07	204.12	0.0528
	H-5 → L+5 (70%)	LMCT/ILCT	6.28	197.59	0.0403
	H-6 → L+7 (23%)	ILCT	6.44	192.59	0.0747
	H-1 → L+16 (10%)	d-d/LLCT/MLCT			
	H-9 → L+6 (22%)	LLCT/IL	6.47	191.80	0.0430
	H-4 → L+10 (15%)	LMCT/IL			
	H-10 → L+3 (11%)	IL			

ϵ – molar absorption coefficient; H – highest occupied molecular orbital; L – lowest unoccupied molecular orbital

Table S15. The energies and characters of the selected spin-allowed electronic transitions for **5** calculated with the TDDFT/B3LYP method, together with assignment to the experimental absorption bands.

Experimental absorption λ ; nm ($10^{-3} \epsilon$; M ⁻¹ cm ⁻¹)	Calculated transitions				
	Major contribution (%)	Character	E [eV]	λ [nm]	Oscillator strength
383.2 (9.5)	H-1 → L (98%)	MLCT/LLCT	3.04	408.34	0.1044
300.5 (46.5)	H-4 → L (63%)	ILCT	3.88	319.63	0.2750
	H-3 → L (68%)	ILCT/IL	3.94	314.37	0.0948
	H → L+2 (51%)	MLCT/LLCT	4.01	309.23	0.1209
	H-8 → L (53%)	LLCT	4.38	283.09	0.0535
	H-3 → L+1 (56%)	ILCT	4.55	272.55	0.1689
260.1 (60.9)	H-3 → L+1 (23%)	ILCT MLCT/LLCT	4.56	271.68	0.1958
	H → L+3 (14%)				
	H-9 → L (12%)	LLCT			
	H-2 → L+4 (31%)	MLCT	4.77	260.23	0.0851
197.4 (125.8)	H-2 → L+3 (17%)	MLCT			
	H-4 → L+7 (36%)	IL/ILCT ILCT/IL	5.94	208.89	0.0514
	H-5 → L+3 (15%)				
	H-13 → L+1 (36%)	IL/ILCT LLCT	6.28	197.37	0.0659
	H-11 → L+2 (14%)				
	H-5 → L+6 (26%)	IL ILCT/LMCT LMCT	6.36	194.94	0.0647
	H-3 → L+8 (21%)				
	H-5 → L+5 (16%)				
	H-3 → L+9 (23%)	ILCT/LMCT	6.49	191.15	0.0803

ϵ – molar absorption coefficient; H – highest occupied molecular orbital; L – lowest unoccupied molecular orbital

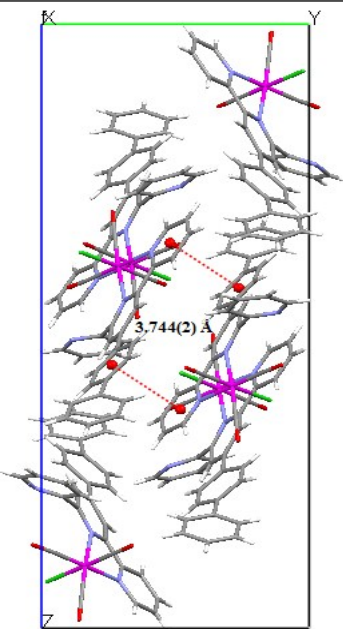
Table S16. The energies and characters of the selected spin-allowed electronic transitions for **6** calculated with the TDDFT/B3LYP method, together with assignment to the experimental absorption bands

Experimental absorption λ ; nm ($10^{-3} \epsilon$; M ⁻¹ cm ⁻¹)	Calculated transitions				
	Major contribution (%)	Character	E [eV]	λ [nm]	Oscillator strength
419.2 (16.5)	H → L (98%)	ILCT	2.54	487.62	0.3663
	H-1 → L (98%)	MLCT/LLCT	3.04	407.41	0.0123
	H → L+1 (96%)	ILCT	3.15	393.40	0.3388
354.1 (9.3)	H → L+2 (98%)	ILCT	3.53	351.70	0.0739
308.7 (14.2)	H → L+3 (89%)	ILCT/LMCT	3.83	323.46	0.0907
	H-4 → L (59%)	IL/ILCT	3.93	315.86	0.1122
	H-2 → L+1 (69%)	MLCT/LLCT	3.98	311.94	0.0754
	H-5 → L (42%)	ILCT/IL	4.07	304.86	0.1067
	H-1 → L+2 (27%)	MLCT/LLCT			
246.2 (17.7)	H-4 → L+1 (56%)	IL	4.73	262.08	0.1767
	H-11 → L (31%)	IL	5.13	241.81	0.0792
	H-3 → L+5 (13%)	MLCT			
	H-6 → L+1 (11%)	IL/LLCT/ILCT			
	H-10 → L+1 (13%)	LLCT/ILCT	5.54	223.89	0.0788
192.2 (178.2)	H-4 → L+9 (23%)	LMCT/IL/ILCT	6.33	195.77	0.0707
	H-13 → L+1 (17%)	IL/ILCT			
	H-9 → L+6 (38%)	LLCT/IL	6.45	192.28	0.0639
	H-11 → L+3 (16%)	IL/LMCT			
	H-4 → L+9 (31%)	LMCT/IL/ILCT	6.47	191.69	0.1285
H-13 → L+1 (14%)	H-13 → L+1 (14%)	IL/ILCT			
	H-9 → L+6 (13%)	LLCT/IL			

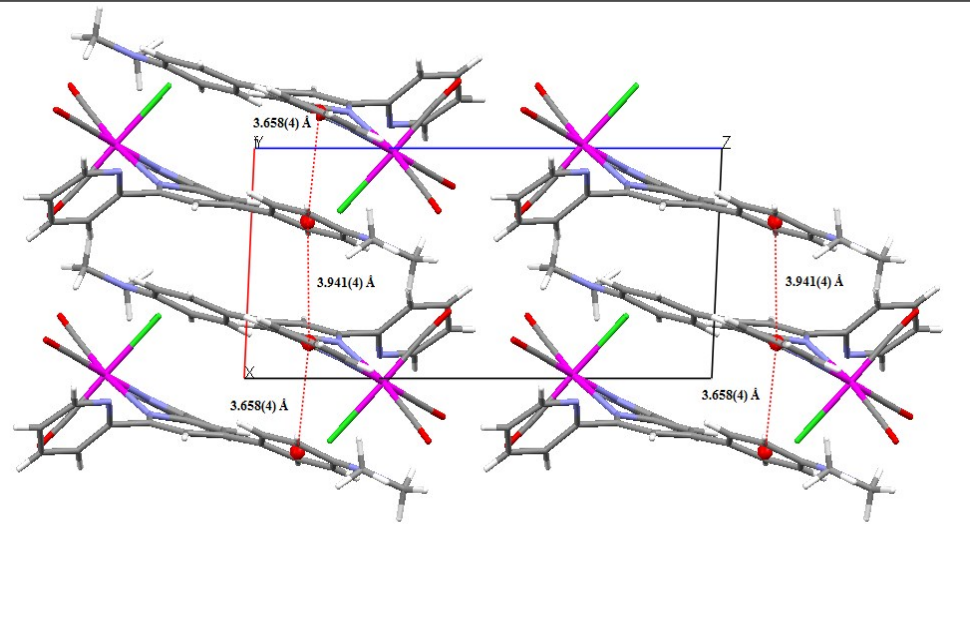
ϵ – molar absorption coefficient; H – highest occupied molecular orbital; L – lowest unoccupied molecular orbital

Table S17. The energies and characters of the two lowest vertical electronic transitions for **6** complex obtained in TDDFT calculations with using different functionals.^a

Solvent	State	E [eV]	λ [nm]	f	Character
B3LYP					
ACN	S ₁	2.54	487.62	0.3663	H → L IL/ILCT
	S ₂	3.04	407.42	0.0123	H-1 → L MLCT
CHCl ₃	S ₁	2.58	481.02	0.3558	H → L IL/ILCT
	S ₂	2.86	433.58	0.0203	H-1 → L MLCT
BP86					
ACN	S ₁	1.80	688.30	0.1849	H → L IL/ILCT
	S ₂	2.36	524.72	0.1474	H → L+1 IL/ILCT
CHCl ₃	S ₁	1.84	673.14	0.1816	H → L IL/ILCT
	S ₂	2.19	566.45	0.0066	H-1 → L MLCT
ω B97					
ACN	S ₁	4.08	303.61	0.9425	H → L IL/ILCT
	S ₂	4.16	297.73	0.1424	H-1 → L H-1 → L+4 MLCT
CHCl ₃	S ₁	4.09	303.46	0.5399	H → L H-1 → L IL/ILCT/MLCT
	S ₂	4.13	299.94	0.4316	H-1 → L H → L MLCT/IL/ILCT
ω B97x					
ACN	S ₁	3.96	313.42	0.9364	H → L IL/ILCT
	S ₂	4.08	304.15	0.1124	H-1 → L MLCT
CHCl ₃	S ₁	3.95	313.86	0.5395	H → L H-1 → L IL/ILCT/MLCT
	S ₂	4.01	308.93	0.3754	H-1 → L H → L MLCT/IL/ILCT
CAM-B3LYP					
ACN	S ₁	3.50	354.43	0.7935	H → L IL/ILCT
	S ₂	3.74	331.72	0.0702	H-1 → L MLCT
CHCl ₃	S ₁	3.50	354.11	0.5606	H → L IL/ILCT
	S ₂	3.61	343.79	0.2192	H-1 → L MLCT
LC-BLYP					
ACN	S ₁	4.14	299.50	0.9031	H → L IL/ILCT
	S ₂	4.24	292.69	0.2125	H-1 → L H-1 → L+4 MLCT
CHCl ₃	S ₁	4.14	299.67	0.5605	H → L H-1 → L IL/ILCT/MLCT
	S ₂	4.21	294.65	0.4475	H-1 → L H → L MLCT/IL/ILCT



1



6

Figure S1. A view of the crystal packing showing intermolecular $\pi-\pi$ stacking interactions for **1** and **6**.

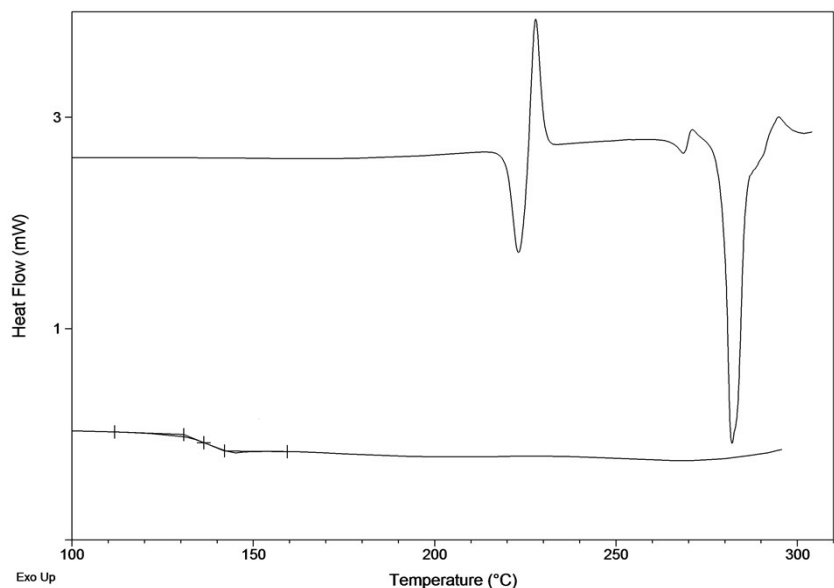


Figure S2. DSC thermograms of compound **2**. T_c : crystallization temperature; T_m melting point temperature; T_g glass transition temperature.

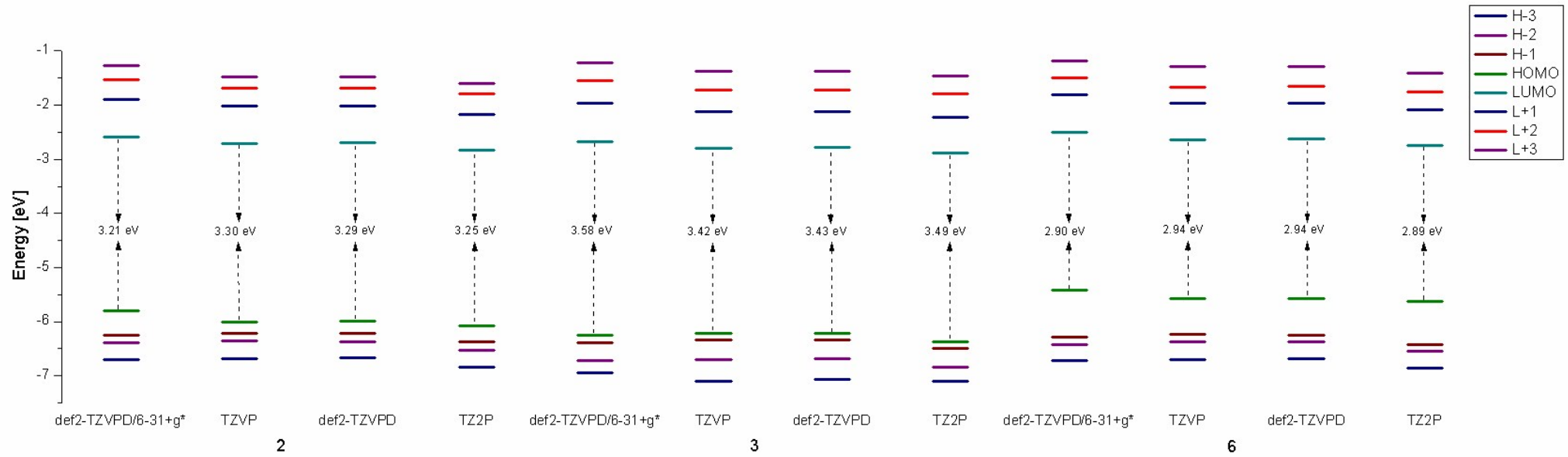
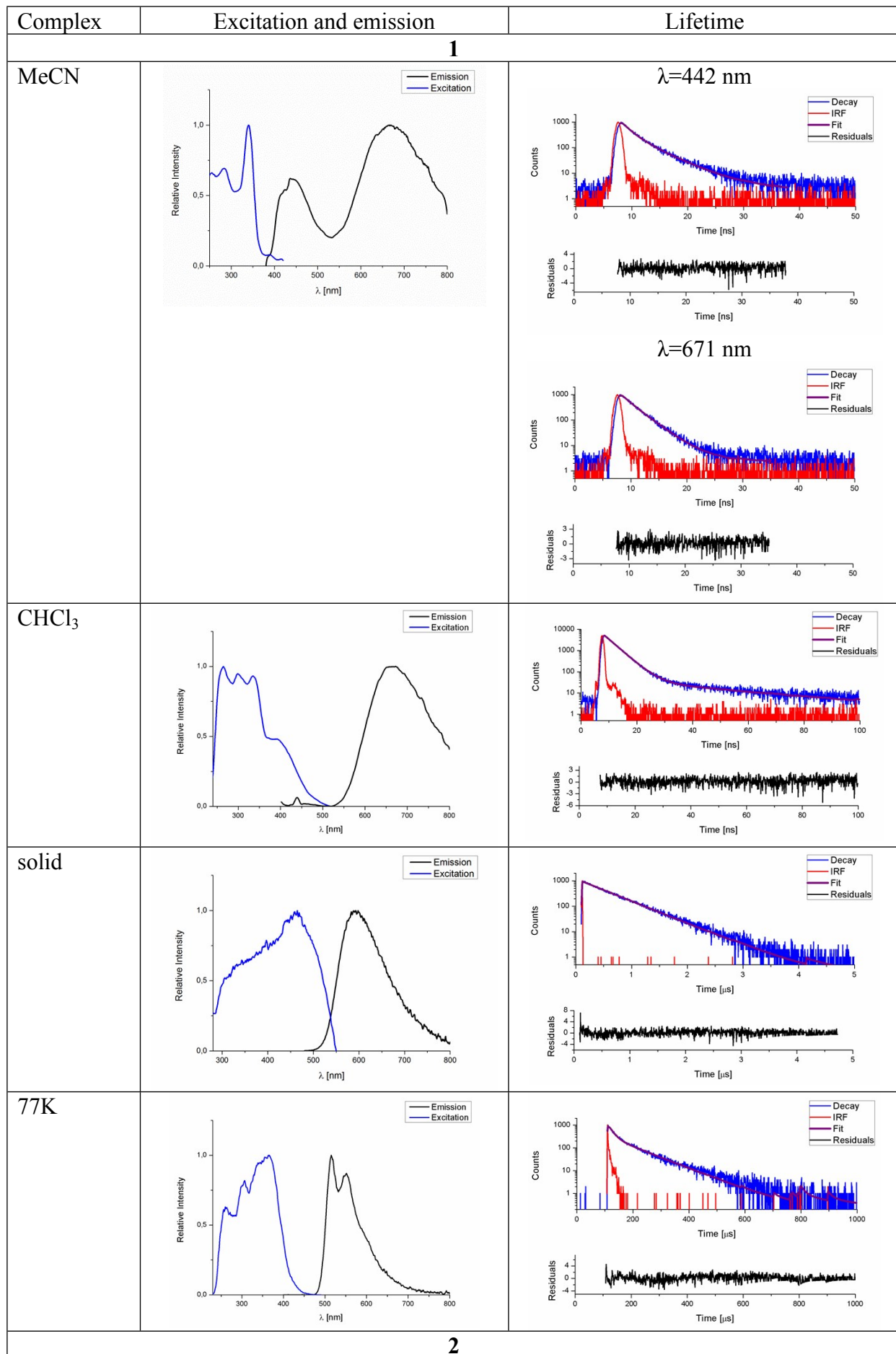
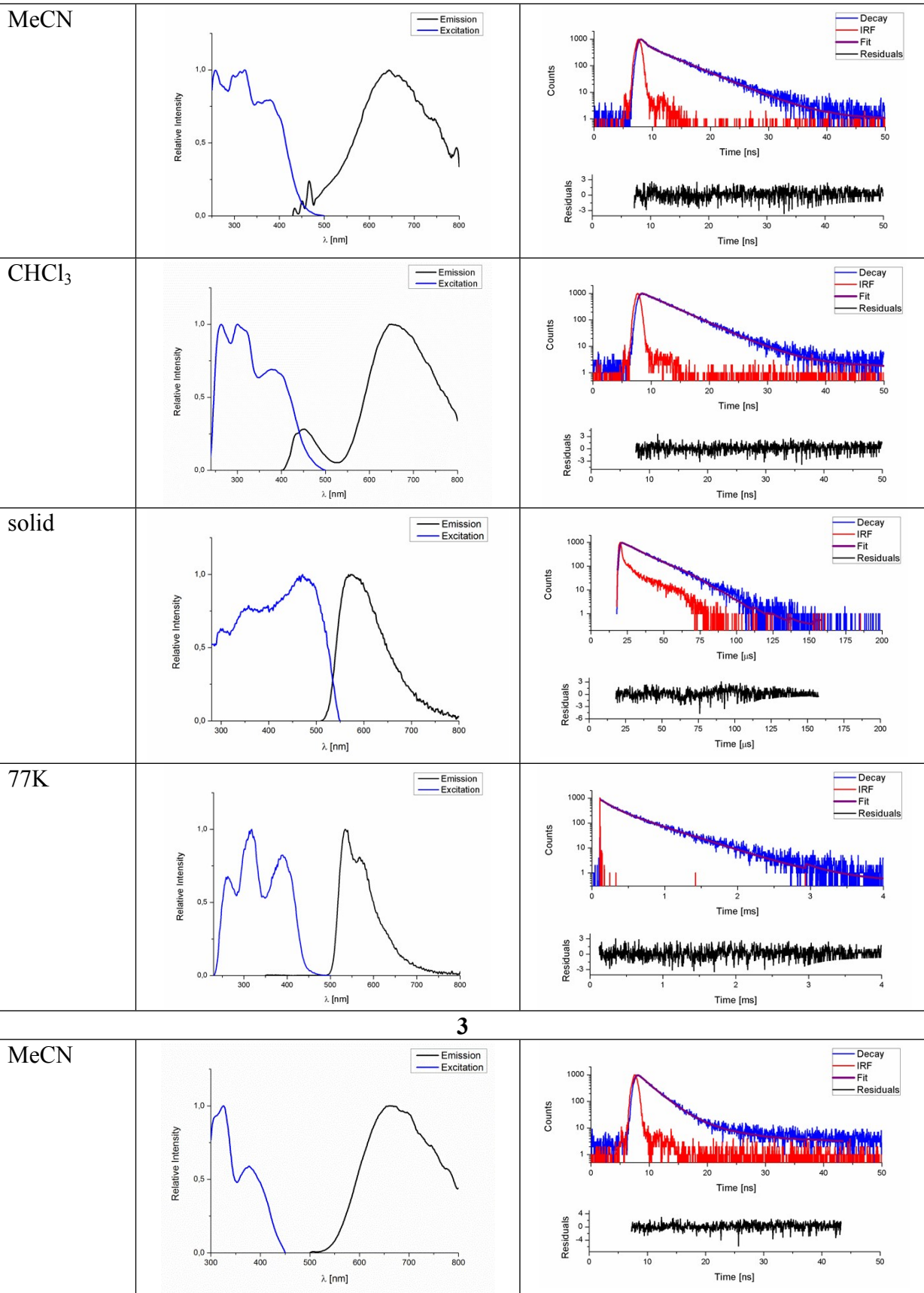


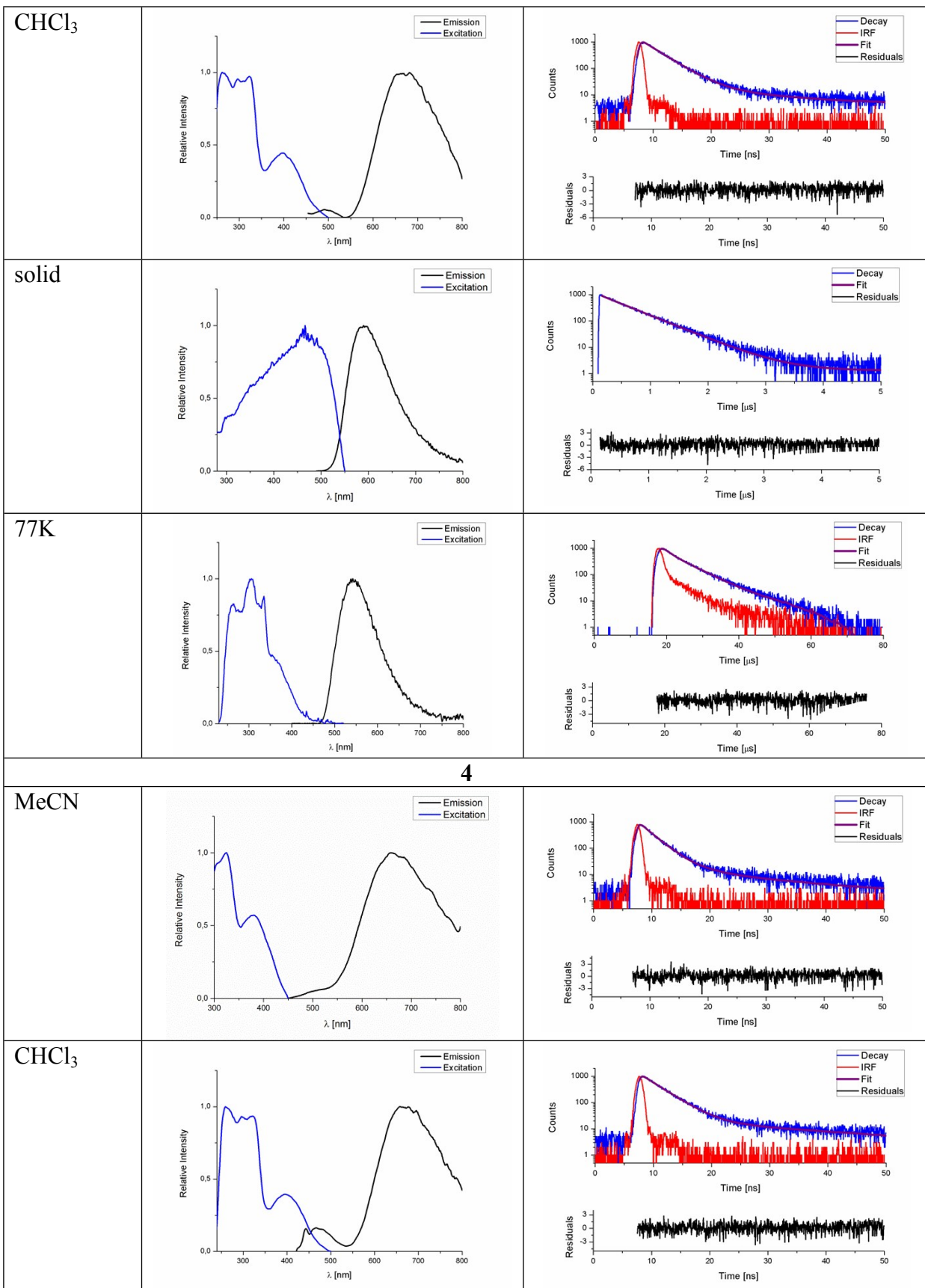
Figure S3. Molecular orbital energy level graph of complexes **2**, **3** and **6** at the DFT/B3LYP level using different basis sets.

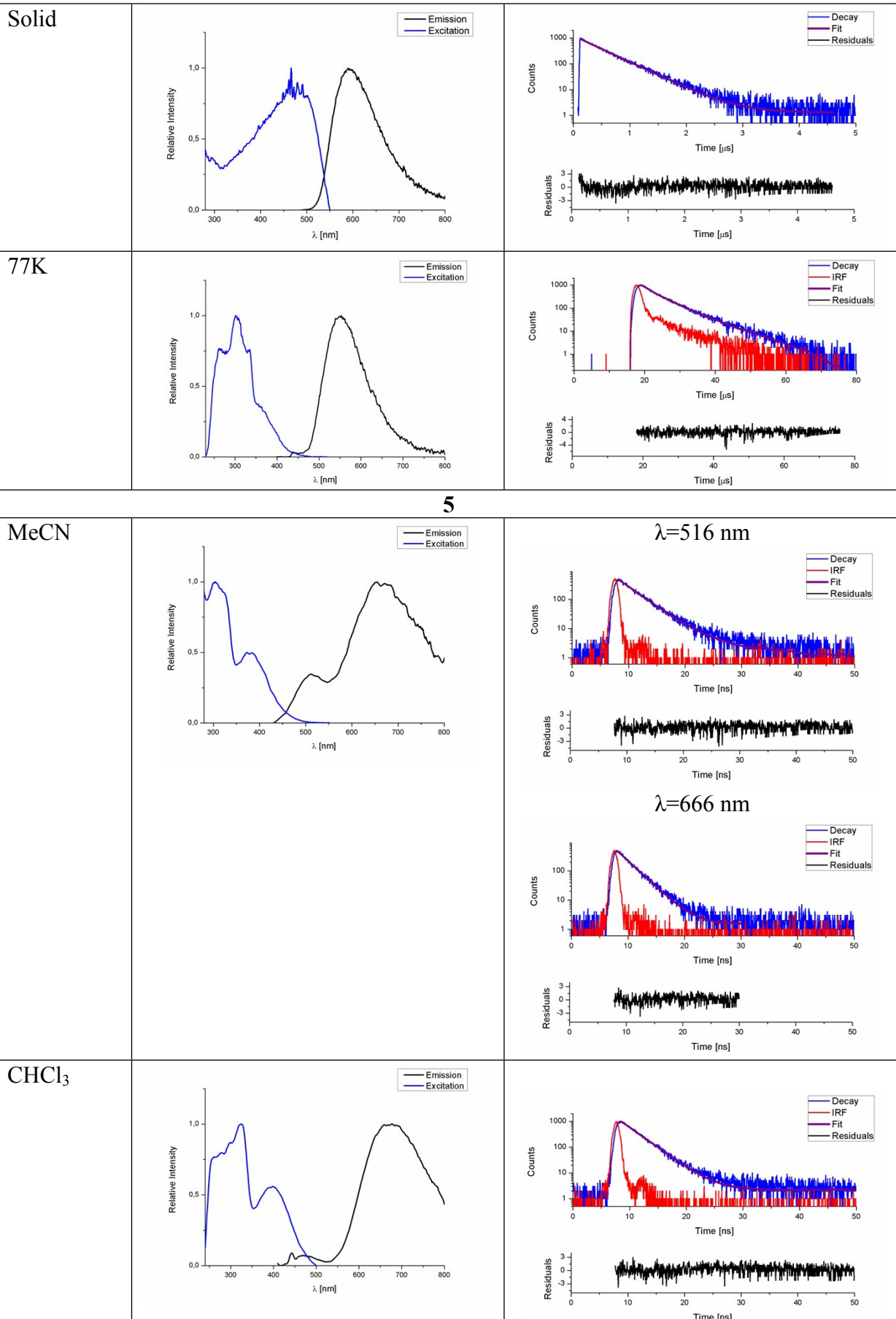


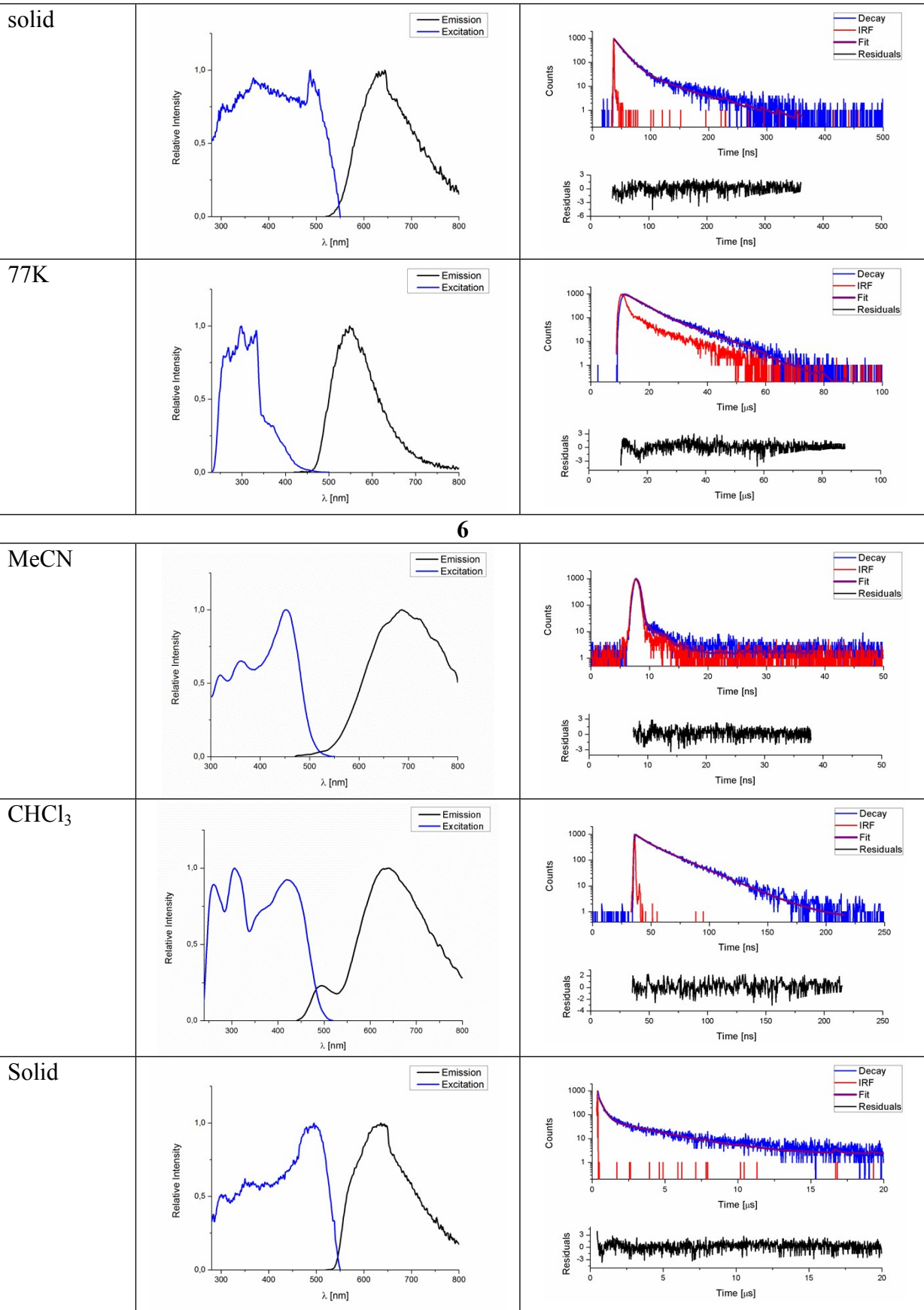
2



3







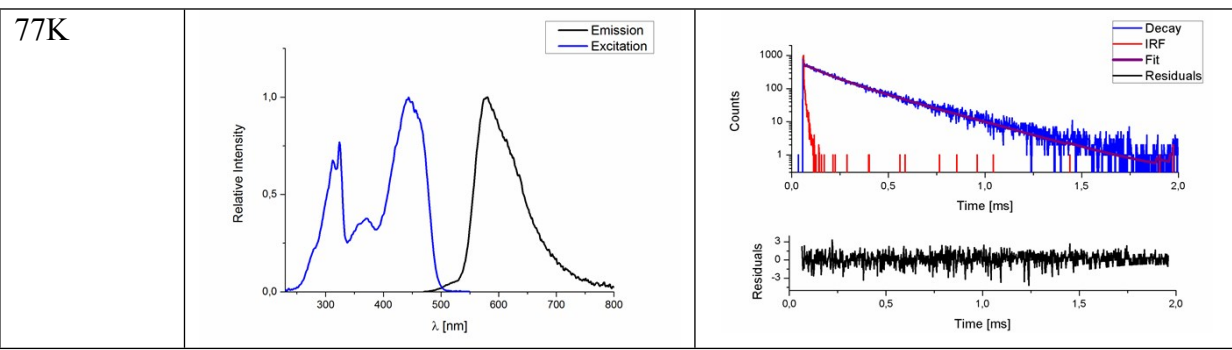
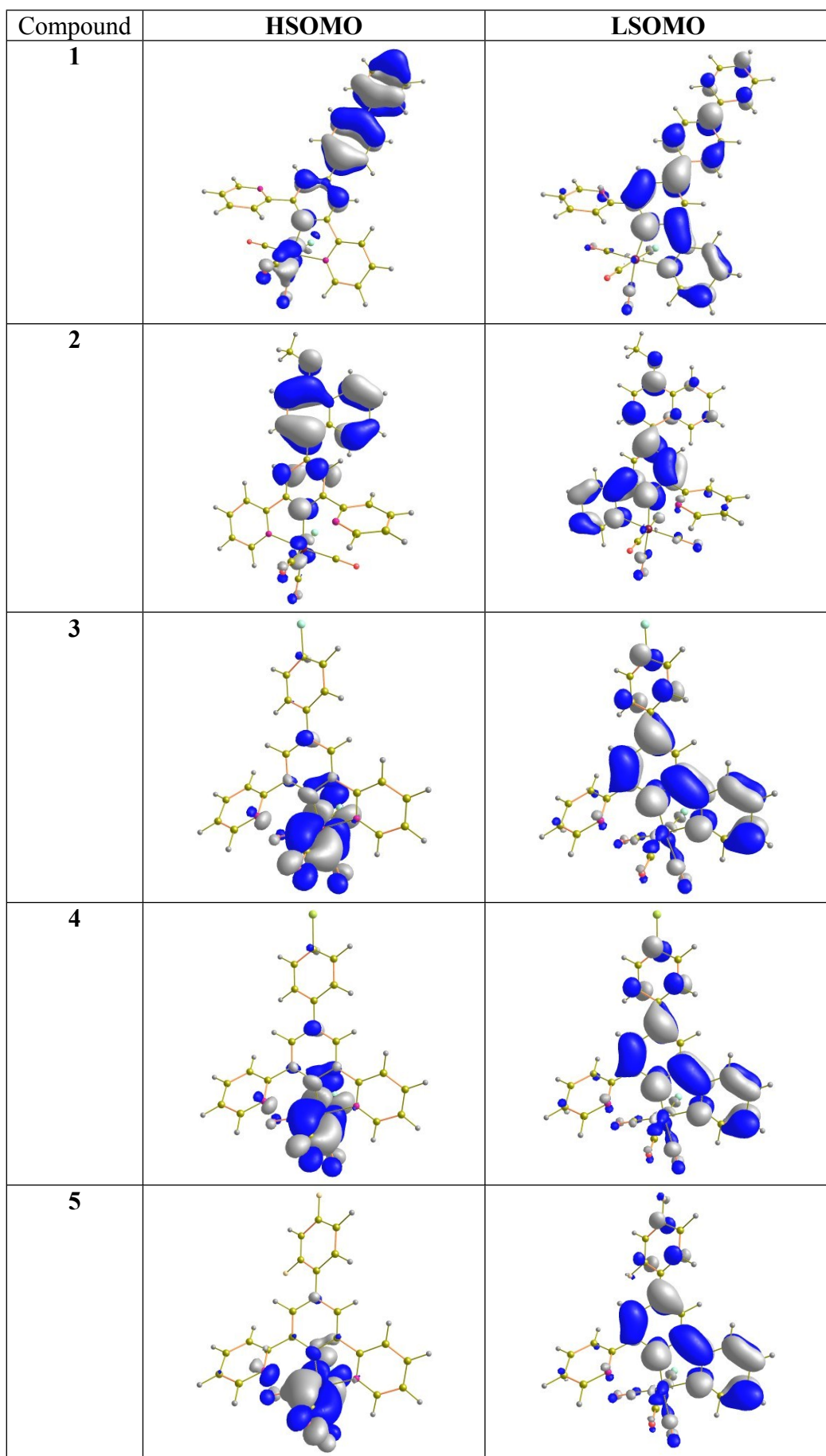


Figure S4 Excitation and emission spectra together with PL lifetime curves for **1-6** in CHCl₃, MeCN, low-temperature MeOH:EtOH glass matrix and in solid state.



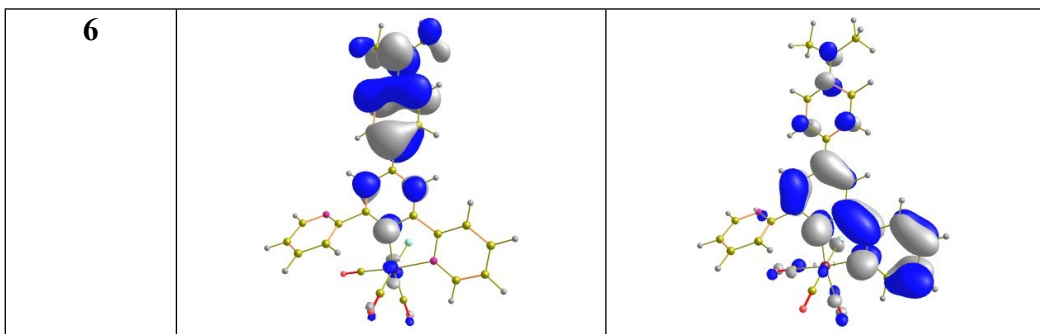


Figure S5. Isodensity surface plots of the HSOMO and LSOMO for the complexes **1–6** at their T₁ state geometry calculated in MeCN medium at the TD-DFT/DFT/B3LYP level associated with the PCM model. Blue and grey colours show regions of positive and negative spin density values, respectively.

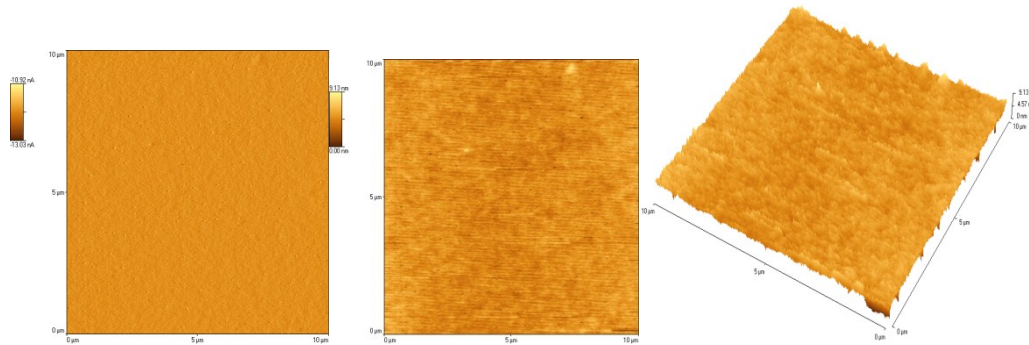


Figure S6. AFM images (10 μm x 10 μm) of the blend PVK with compound **3**